

Title: Multiplex movie of concerted rotation of molecules on a 2D material

Authors: Kiana Baumgärtner¹, Misa Nozaki², Marvin Reuner³, Nils Wind^{4,12}, Masato Haniuda², Christian Metzger¹, Michael Heber⁵, Dmytro Kutnyakhov⁵, Federico Pressacco⁵, Lukas Wenthaus⁵, Keisuke Hara², Chul-Hee Min⁶, Martin Beye⁵, Friedrich Reinert¹, Friedrich Roth^{7,8}, Sanjoy Kr Mahatha^{5,9}, Anders Madsen¹⁰, Tim Wehling^{3,11}, Kaori Niki², Daria Popova-Gorelova^{3,11}, Kai Rossnagel^{6,12,13}, Markus Scholz^{5,10*}

Affiliations:

¹Experimentelle Physik 7 and Würzburg-Dresden Cluster of Excellence ct.qmat, Julius-Maximilians-Universität, Am Hubland, 97074 Würzburg, Germany

²Graduate School of Science and Engineering, Chiba University, 1-33 Yayoi-cho, Inage-ku, Chiba 263-8522, Japan

³I. Institute for Theoretical Physics and Centre for Free-Electron Laser Science, Universität Hamburg, Luruper Chaussee 149, 22607 Hamburg, Germany

⁴Institut für Experimentalphysik, Universität Hamburg, Luruper Chaussee 149, 22761 Hamburg, Germany

⁵Deutsches Elektronen-Synchrotron DESY, Notkestraße 85, 22607 Hamburg, Germany

⁶Institut für Experimentelle und Angewandte Physik, Christian-Albrechts-Universität zu Kiel, Olshausenstraße 40, 24098 Kiel, Germany

⁷Institute of Experimental Physics, TU Bergakademie Freiberg, Leipziger Straße 23, 09599 Freiberg, Germany

⁸Center for Efficient High Temperature Processes and Materials Conversion (ZeHS), Winklerstraße 5, 09599 Freiberg, Germany

⁹UGC-DAE Consortium for Scientific Research, Khandwa Road, Indore 452001, Madhya Pradesh, India

¹⁰European X-Ray Free-Electron Laser Facility, Holzkoppel 4, 22869 Schenefeld, Germany

¹¹The Hamburg Centre for Ultrafast Imaging (CUI), Luruper Chaussee 149, 22607 Hamburg, Germany

¹²Ruprecht Haensel Laboratory, Deutsches Elektronen-Synchrotron DESY, Notkestraße 85, 22607 Hamburg, Germany

¹³Kiel Nano, Surface and Interface Science KiNSIS, Kiel University, Christian-Albrechts-Platz 4, 24118 Kiel, Germany

*To whom correspondence should be addressed; markus.scholz@desy.de.

Abstract

Function is dynamic and originates at atomic interfaces. Combining the degrees of freedom of molecules (1,2) with the peculiar properties of 2D quantum materials (3,4,5) can create novel functionality (6,7). Here, we report the manipulation and ultrafast imaging of a unidirectional gearing motion in molecules on a 2D quantum material. To visualize and disentangle the

intertwined structural and electronic dynamics of such a hybrid interface, we record a ‘full molecular movie’ (8) by imaging the atomic positions (9,10), the evolution of the molecular orbital wavefunctions (11,12) and the modification of electronic states of the substrate (13). In a multimodal investigation in a single setup (14), we disentangle dynamics in valence and core electrons of both the molecule and the surface with femtosecond and sub-ångström precision. The ultrafast rotational motion is fueled by the transfer of hot holes into the molecules that results in “supercharging” of the film. As hot carriers move through the interface, we track a transient modification of the frontier molecular orbitals and observe a chiral symmetry breaking associated with local structural rearrangements. Our calculations show that the “supercharging” changes the interfacial potential energy landscape and triggers the gearing motion. The experiment offers all-in-one imaging of the electronic, molecular orbital, chemical and structural dynamics during the flow of charge and energy across the hybrid interface. Our approach provides detailed dynamical information on the mechanism underlying surface-adsorbed molecular gears and enables tailoring novel functionalities in hybrid active matter.

Main

New functionality can arise at engineered atomic interfaces between functional molecular systems and solid surfaces. Prototypical examples are molecular switches that rely on their ability to harness an external stimulus, e.g., optical, chemical, or electrical, and convert it to mechanical motion (15). Such molecular systems can be tailored to function like a gearbox composed of two molecules rotating against each other. Various strategies have been used to control gear-like rotation on surfaces, but most have focused on isolated rotor structures. In such molecular rotors, gear-like motion can be triggered by external stimuli such as an electric field through a scanning tunneling microscopy tip (1,2).

Synchronized and unidirectional gearing motion in a large ordered 2D ensemble, however, requires more complex designs (16). Molecular systems adsorbed on 2D quantum materials provide a particularly suitable platform to customize the potential energy surface that governs and controls the structural response of the interface. At such hybrid interfaces driven far from equilibrium, hot charge carriers generated after optical excitation can be injected from the 2D quantum material into the molecules on an ultrafast (femtosecond) time scale, triggering a structural response in a 2D array on macroscopic length scales (17). This opens up the possibility of efficient energy transfer across the surface, which is required for the assembly of large-scale cooperating molecular machines.

It has been a long-standing goal of surface and interface science to record molecular movies with a single experimental setup (14). Here, such a multiview experiment is realized by integrating four modalities of time-resolved photoelectron spectroscopy—time-resolved orbital tomography, trARPES, trXPS, and trXPD (time- and angle-resolved photoemission spectroscopy, time-resolved X-ray photoelectron spectroscopy and time-resolved X-ray photoelectron diffraction, respectively)—using ultrashort-pulsed extreme ultraviolet and soft x-ray radiation for valence- and core-electron emission.

The goal is to initiate a gearing motion in Copper(II)phthalocyanine (CuPc) molecules in a self-assembled, highly ordered molecular film adsorbed on the transition-metal dichalcogenide TiSe₂ (Fig. 1). In the following, we show that more than half of the molecules become positively charged by hot carrier injection from the 2D material into the adsorbates. Our calculations show that such

“supercharging” of the molecular film significantly changes the interfacial potential energy landscape and triggers gearing motion in a large ensemble of molecules. This is a far more efficient method than manipulating individual molecules with a scanning tunneling microscope, as shown previously (1,18,19). Since the formation of long-range order in self-assembled organic films is controlled by both molecule-substrate interactions and intermolecular interactions, a structural response of the molecules is initiated that adapts to the new energy landscape (Fig. 1). The combination of four modalities of time-resolved photoelectron spectroscopy allows us to monitor this structural response and to correlate it with the charge and energy flow across the hybrid interface.

Energy flow and supercharging

First, the charge and energy flow fueling the collective rotational motion of the molecules is explained by linking the population dynamics of the molecular orbitals to the nonequilibrium population dynamics of the electronic states in TiSe₂ around the Fermi level (E_F). By means of orbital tomography we can identify individual molecular orbitals (Fig. 2 a,c) by their intensity distribution in momentum space, disentangle the signature of the molecular wavefunction from the substrate states, and follow the energy flow between molecule and substrate in time (12).

Upon optical pumping of TiSe₂ (at time t_0), spectral weight is redistributed from the Se 4*p* valence band (Fig. 2 d) into the Ti 3*d* conduction band (Fig. 2 b) (3,4). Immediately thereafter, hot electrons start to relax to higher binding energies into the Ti 3*d* conduction band minimum by intraband scattering, and hot holes scatter to lower binding energies into the Se 4*p* valence band maximum (Fig. 3 a and b). Because of the proximity of the CuPc highest occupied molecular orbital (HOMO, Fig. 2 c) to E_F , hot holes are eventually injected into the molecule within ~375 fs after absorption of the pump pulse (t_1). As a result of hot hole transfer, about 45% (cf. trXPS analysis below) of the adsorbed molecules become positively charged (CuPc_{*t*₁}⁺) leading to a “supercharging” of the molecular film. This results in an electrostatic potential energy difference, both with respect to the substrate and to the remaining neutral molecules (CuPc_{*t*₁}⁰) and can be qualitatively understood in terms of classical electrostatics (20). As a result, all energy levels shift toward E_F , reaching a maximum shift of ~200 meV at t_1 (Fig. 3 c). The lowest unoccupied molecular orbitals (LUMO and LUMO', Fig. 2 a) are also transiently populated at t_0 , but play only a minor role in modulating the interfacial potential landscape since their intensity suggests that only ~1% of the molecules are excited into this state. We have summarized the charge carrier dynamics schematically in Fig. 2 e.

To confirm the role of hot hole transfer in modulating the interfacial potential, the ratio of CuPc_{*t*₁}⁺ to all molecules at t_1 (CuPc_{*t*₁}) is quantified with trXPS (Fig. 3 d) (9,10,21). First, the spectral signatures of CuPc_{*t*₁}⁺ (red) and CuPc_{*t*₁}⁰ (blue) molecules are identified in the carbon 1*s* (C 1*s*) core-level signal by comparison with calculations (20) (Fig. 3 e). We find that the spectrum of CuPc_{*t*₁}⁺ is shifted toward higher binding energy compared to before excitation (CuPc_{*t*₁}), which is due to reduced core-hole screening during the transfer of hot holes from the Se 4*p* band to the HOMO (see Methods and (20) for peak assignments and fits). By contrast, the signature of CuPc_{*t*₁}⁰ is rigidly shifted toward lower binding energy due to modulation of the surface potential (see Methods and (20)). From the relative peak intensities, we estimate the maximum ratio of CuPc_{*t*₁}⁺ / CuPc_{*t*₁} to be ~45% indicating that about every second molecule is charged.

Structural dynamics from wavefunction and XPD pattern analysis

During this transient phase of the supercharged molecular film, a gearing motion of cogwheel pairs of CuPc molecules is observed, i.e., a synchronized clockwise (CW) and counter-clockwise (CCW) rotation of CuPc⁰ and CuPc⁺ molecules, respectively (see Fig. 1). The ultrafast cogwheel rotation is observed in both tomographic snapshots of the HOMO (Fig. 4 a) and photoelectron diffraction patterns of the C 1s core level (Fig. 4 b, c) within ~375 fs after absorption of the pump pulse.

The electron density distribution of the HOMO is represented by a ring-like structure with 12 distinct peaks (α) in momentum space (Fig. 4 a). Both a CCW and a CW rotation of the HOMO are observed at t_1 . This manifests itself in two additional peaks (β , γ) appearing at azimuthal positions of about $-15^\circ \pm 3^\circ$ and $+15^\circ \pm 3^\circ$, respectively. Ionization of CuPc⁺ results in a modification of the HOMO shape. In momentum space, the γ peak shifts toward the Γ -point by about 0.1 \AA^{-1} . This is consistent with our calculation of the shape change of the ionized CuPc HOMO (see Methods and (20)) and thus allows the unambiguous assignment of the β and γ peaks to CuPc⁰ and CuPc⁺, respectively.

Similar to the tomographic HOMO snapshots, we deduce a CCW and CW rotation for CuPc⁺ and CuPc⁰, respectively, from the atomic positions of the carbon atoms. The distinct spectral fingerprint in the C 1s spectra of neutral and charged molecules allows us to disentangle the atomic rearrangement for each species. The C 1s trXPD patterns of neutral and charged molecules consist of 6 and 3 distinct peaks, respectively. The calculations show that these dominant features are the result of intramolecular scattering. Fig. 4 b shows the trXPD pattern and the analysis of the neutral molecules before and after t_0 . The main features are marked with δ and ϵ in the upper left inset. An azimuthal line cutting through δ and ϵ reveals a CW rotation of about $-15^\circ \pm 3^\circ$ of the neutral molecules (CuPc⁰) after t_0 . In addition, δ' and ϵ' for CuPc⁰ appear shifted toward the Γ -point. Our calculations suggest that this is related to a decreased adsorption height at t_1 . The charged CuPc⁺ molecules are rotated CCW by about $+15^\circ \pm 3^\circ$, as shown by comparison with the calculated pattern (Fig. 4 c). Moreover, the trXPD pattern of CuPc⁺ is strongly modified, indicating deformation of the molecules after hot hole transfer. XPD calculations on a series of model geometries show out-of-plane deformation, with benzene wings approaching the substrate (Fig. 4 d). Not all molecules are rotated at t_1 : In both the tomographic snapshots of the HOMO and the trXPD patterns, we also detect the signature of nonrotating molecules. According to our analysis of the trXPD pattern of CuPc⁰, about 40% of the neutral molecules do not rotate. A similar fraction is estimated from the signal of the charged species CuPc⁺, but the quantification is subject to an error of $\pm 10\%$ because the trXPD pattern of CuPc⁺ is superimposed on the signature of nonrotating CuPc⁰ (Fig. 4 e).

The CCW and CW rotations are driven by the changed intermolecular interactions between charged and neutral molecules between t_0 and t_1 . We calculate the pair potential between the molecules using partial charges on each atom in the molecules obtained from the RASSCF calculation of the ground state of CuPc_{*t*-1} and the ionized state of CuPc_{*t*-1}⁺ (20). Such a pair-potential calculation was previously applied to similar molecular systems (22–24). As a result, it is found that depending on}

the initial in-plane orientation of the molecules relative to their unit cell (angles marked in Fig. 4 f, g), CuPc_1^+ and CuPc_1^0 molecules adapt to the new potential energy surface and consequently rotate in CCW and CW directions, respectively.

Interestingly, we observe unidirectional motion of the molecules despite the existence of mirror domains immediately after sample preparation, as shown by our low-energy electron diffraction (LEED) measurements. In mirror domains, molecules should exhibit reversed rotations, as suggested by our pair-potential calculations, but this is not evident in the experimental data. This may indicate that molecular reorganization has occurred over the measurement time, resulting in the suppression of mirror domains and the formation of extended homochiral domains. Homochirality in large molecular systems is observed in nature and often linked to spontaneous symmetry breaking (25). Even for achiral molecules, mirror symmetry can be broken by distortions of the molecules during adsorption (26, 27) or by asymmetric charge transfer (28), which can ultimately lead to homochirality on the entire surface (29–31).

In our system, the out-of-plane deformation of CuPc_1^+ breaks the four-fold symmetry of CuPc into a two-fold one. In addition, the nearly square molecular unit cell (Fig. 4 f) suggests that there is only a small potential barrier between domain and mirror domain (Fig. 1). We therefore assume that the recurrent modulation of the interfacial potential during the experiment provided sufficient energy to shift the system toward extended homochiral domains. Based on our combined experimental observations and pair-potential calculations, we derive the molecular arrangements shown in Fig. 4 f and g.

Conclusion

In summary, we have realized and observed ultrafast concerted gearing motion of achiral cogwheel pairs on a 2D quantum material. The unidirectional rotation is initiated by charge carrier transfer between substrate and molecules and guided by the potential energy surface, which adapts to the changing charge distribution at the hybrid interface far from equilibrium. The reduced symmetry of the charged molecules acts as chiral perturbation and seeds the creation of domains with a unidirectional rotation. The multimodal time-resolved orbital tomography, trARPES, trXPS, and trXPD approach allows us to link information about the global interfacial electronic dynamics with local atomic site-specific information about the charge state dynamics and relate it to the ultrafast deformation and rotation of the molecules. This novel direct, microscopic, and multi-perspective insight into the interplay between structural and electronic dynamics will enable better understanding and control of molecular machines on surfaces. We see this as a prerequisite for the rational design of new functionalities in hybrid active matter.

Methods

Experimental conditions

The experiments for the CuPc/TiSe₂ valence band structure were performed at both a HHG and FEL source, with pump excitation energy of 1.6 eV and probe pulse energy of 36.3 eV (both p-polarized). Both experiments result in the same observed dynamics, but due to longer acquisition times and thus better statistics, we chose to present the valence band data acquired at the HHG source in the main manuscript (32). The experiments for the C 1s core level were performed at the

PG2 beamline at FLASH in Hamburg, Germany, with a pump energy of 1.6 eV and probe energy of 370 eV. Pump and probe pulses impinge at a polar angle of 68° and an azimuthal angle of 0° with respect to the substrate's Γ -M direction on the sample. The spot sizes of the pump and probe beams on the sample are about $(260 \times 150) \mu\text{m}^2$ and $(200 \times 100) \mu\text{m}^2$ and both beams are aligned to have spatial overlap. The average FEL pulse energy of $30 \mu\text{J}$ is attenuated by several thin-film filter foils and by nitrogen gas. The pump laser provides a maximum flux of $1 \text{ mJ}/\text{cm}^2$. The energy resolution of the experiment is 80 meV as evaluated from fitting the Fermi edge of an Ag(110) crystal at room temperature. The temporal resolution is (95 ± 5) fs for the valence band data taken at the HHG source and (180 ± 10) fs for the core level data taken at the FEL source, as evaluated from the pulses' cross-correlation. The photoelectrons are detected by a time-of-flight momentum microscope (14). The data-sets sampling over ~ 2 ps were acquired in ~ 15 h. The energy of the obtained spectra is calibrated by comparison of the central CuPc HOMO energy with a value previously measured at a He-I source using a hemispherical analyzer (Scienta Omicron R3000). The momentum maps are similarly calibrated at the Γ -points of a clean TiSe₂ sample. All shown momentum maps are integrated over ± 220 meV around the denoted center energy and are three-fold symmetrized according to the substrate symmetry. No further data treatment was performed.

Sample preparation

The CuPc monolayer on TiSe₂ was prepared *in situ* at a base pressure of 10^{-10} mbar. The TiSe₂ substrate of $\sim (5 \times 5) \text{ mm}^2$ size was cleaved *in situ* and characterized by low-energy electron diffraction (LEED) and photoemission measurements prior to the deposition of molecules. CuPc molecules (gradient sublimated) were deposited via organic molecular beam epitaxy from a home-made Knudsen-cell evaporator at a Knudsen cell temperature of 400 K and a deposition rate of 1 monolayer per 40 min at an evaporator-to-sample distance of 15 cm. These growth parameters were previously determined by means of LEED and photoemission measurements on CuPc molecules deposited on an Ag(110) crystal with a well-characterized growth. The LEED image characteristic for a monolayer of CuPc molecules on TiSe₂ is shown in Extended Data Fig. 1 and a molecular superstructure of $(2, 4.5/4, 0.2)$ is determined. From this superstructure a real-space arrangement of densely packed flat-lying molecules with a distance of 13.8 \AA can be determined. During the beamtime, several samples were prepared and their quality was verified by LEED.

Time-resolved orbital tomography analysis

Below the Fermi level centered at a binding energy of 310 meV, we identify the CuPc HOMO from its intensity distribution in momentum space. The orbital is characterized by an intensity modulated ring centered around the Γ -point with a radius of $(1.67 \pm 0.01) \text{ \AA}^{-1}$. The calculation of a CuPc molecule adsorbed on a $(8 \times 8 \times 8)$ cluster of TiSe₂ (Fig. 2 c) is performed based on DFT calculations using the Vienna Ab Initio Software Package (VASP). The calculations of the ground state and excited states of a neutral and positively-charged isolated CuPc molecule have been performed with the MOLCAS package (33) using the RASSCF method (34). Further details on the calculation are given in the Supplementary Materials.

At t_0 and between 550 and 990 meV, we identify the CuPc LUMO that is depopulated with a decay time of $\tau_{\text{LUMO}} = (92 \pm 50)$ fs. Its momentum distribution (Fig. 2 a) shows intensity close to the Γ -point stemming from Ti $3d$ states as well as ring-shaped intensity centered around the Γ -point with a radius of $(1.60 \pm 0.05) \text{ \AA}^{-1}$. This is supported by comparison with the calculated momentum distributions of the lowest unoccupied molecular orbitals (LUMO and LUMO') of isolated CuPc, which are overlaid on the experimental data as $1/2 \text{ LUMO} + \sqrt{3}/2 \text{ LUMO}'$. Two excitation

mechanisms can play a role in the transient LUMO population: a direct excitation from HOMO to the LUMO corresponding to an optical gap of ~ 1.1 eV, which is slightly smaller than the reported 1.4 eV for thin films on a metal substrate (35). Due to the off-resonant excitation and the momentum distribution of the $(1/2 \text{ LUMO} + \sqrt{3}/2 \text{ LUMO}')$, we consider the most probable excitation channel to be via hot electron scattering from the Ti 3d band into the LUMO. More details on the LUMO calculations are given in the Supplementary Materials.

Time-resolved XPS analysis

The C 1s core level of the neutral CuPc molecule on TiSe₂ consists of two main peaks and their shake-up satellites. We performed calculations of the C 1s XPS spectra of neutral CuPc and positively-charged CuPc⁺ making use of the extended Koopmans theorem (36). The calculation reproduces the spectrum without the shake-up satellites, but overestimates the separation between the peaks. We determine from the calculation of neutral CuPc that the peak at lower binding energy emerges from the carbon atoms in the benzene rings, while the peak at higher binding energy emerges from the carbon atoms in the pyrrole rings in agreement with literature (37). The calculated C 1s spectrum of positively-charged CuPc⁺ has also two peaks, but the structure of the spectrum changes. The separation between the benzene peak and the pyrrole peak increases by 1 eV. In addition, the benzene peak becomes broader and less intense. The calculated hole density of CuPc⁺ is mainly located on carbon atoms in the pyrrole rings. These atoms experience a stronger decrease of the Coulomb screening than atoms in the benzene rings. This results in the larger shift of the pyrrole peak compared to the shift of the benzene peak toward higher binding energies. A small part of the positive charge is also located on carbon atoms in the benzene rings, but is non-uniformly distributed over these atoms. As a result, carbon atoms in the benzene rings experience a slightly different decrease of Coulomb screening so that the corresponding peak becomes broader.

The C 1s spectra after time zero (t_0) contain the signatures of both neutral and positively charged molecules. In order to determine the ratio of the contributions of the spectra of neutral CuPc and positively-charged CuPc⁺ to the total spectrum, we fitted the total spectrum by adding the two calculated spectra in different ratios. For better comparison, we fitted the global positions of the spectra and decreased the overestimated peak separation by the same value for both spectra. We obtain that the total spectrum is reproduced best, when about 50 % of positively-charged molecules contribute to the spectrum.

Time-resolved XPD calculations and analysis

The XPD data in Fig. 4 b and c show the C 1s signal of CuPc/TiSe₂ after subtraction of the inelastic background. To extract the molecular geometries at t_{-1} and at t_1 , the experimental momentum maps are compared to simulated momentum maps of 42 different sample geometries. Their quantitative agreement is evaluated by means of a R-factor analysis according to the procedure shown in (9). The 42 evaluated R-factors are shown in the Supplementary Materials and the models corresponding to the smallest R-factor are viewed as the closest fits to the experiment (shown in Fig. 4 d).

The simulated models consider one CuPc molecule adsorbed on a cluster of 58 atoms of 1T-TiSe₂ in its normal phase. The different geometrical models of CuPc⁺_{t1} and CuPc on TiSe₂ included varying molecular out-of-plane distortions, adsorption heights, adsorption sites, and molecular in-plane rotations. For each model, three molecular orientations along the substrate high-symmetry

directions according to the point-on-line growth are considered and their intensities for the resulting XPD momentum map are added. The shown XPD momentum maps sum over the intensities stemming from all carbon atoms that are located in the benzene rings. According to the experimental data treatment, the calculated data is three-fold symmetrized. The calculations include multiple scatterings of photoelectrons and are based on Fermi's Golden Rule adopting the Lippman Schwinger equation for the final state (38). Both intramolecular scatterings of CuPc and scatterings at the substrate are considered. The atomic orbitals of the C 1s atoms representing the initial states are calculated by Gaussian (39). Further details on the calculations are provided in the Supplementary Materials.

Fluence dependence

Extended Data Fig. 2 a shows the CuPc C 1s core level for different pump fluences. Since the spectral shape of the C 1s core level does not change when almost doubling the excitation fluence from 0.5 mJ/cm² to 1.2 mJ/cm², we conclude that the observed dynamics are not fluence dependent within the studied region. In the Ti 3d conduction band, efficient hot hole transfer into the CuPc adsorbates is represented by a prolonged population increase after t_0 . In order to evaluate whether the efficient hot hole transfer depends on the pump laser fluence or on the adsorbate coverage, three samples with varying adsorbate coverages are studied for different excitation fluences (see Extended Data Fig. 2 b). Doubling the excitation fluence on pristine TiSe₂ does not impact the Ti 3d population dynamics. TiSe₂ covered by ~0.2 monolayers CuPc also follows the same dynamics as pristine TiSe₂. Only for the TiSe₂ sample covered by a monolayer of CuPc, a prolonged increase of the Ti 3d population is observed.

Dielectric model of the photoexcited system

The excitation-induced binding energy shifts of CuPc- and TiSe₂-derived states toward E_F are modeled by a dielectric model. We assume that a hole is transferred from TiSe₂ to a certain fraction of CuPc molecules. Hence, this fraction will be positively charged, while the rest of the molecules will remain neutral. The substrate carries the opposite negative charge. To describe the dielectric screening in this setup, the CuPc molecules are represented as a dielectric layer ($\epsilon_1=4$, (40)) of thickness $h=3.95$ Å. The TiSe₂ substrate is modeled as a half-space with dielectric constant ϵ_2 , while we assume vacuum above the CuPc layer ($\epsilon_3=1$). For the electron-doped substrate, we consider $\epsilon_2=60$ (41) and, most simplistically, a perfect metal $\epsilon_2=\infty$. The CuPc molecules are assumed to form a square lattice with lattice constant $a=14.5$ Å and the positively charged molecules are modeled as a Gaussian surface charge density of width=5 Å leading to a total charge of +1e. The resulting electrostatic potential is calculated following refs. (42,43) and qualitatively captures the excitation-induced relative level shifts seen in experiment. More details on the calculation are provided in the Supplementary Materials.

Theoretical description of the molecular in-plane orientations

Pair-potential calculations (22) were performed in order to determine the in-plane orientations of molecules at t_{-1} and t_1 . A 2D layer of CuPc molecules is modeled based on the molecular superstructure determined by LEED. The potential in the molecular film is calculated considering intramolecular van-der-Waals and Coulomb interactions. By gradually varying the relative in-plane orientation between a central molecule and its surrounding neighbors, the molecular arrangement

corresponding to the minimum pair-potential is found. More details on the calculations are given in the Supplementary Materials.

References and Notes:

1. D. Peller, L. Z. Kastner, T. Buchner, C. Roelcke, F. Albrecht, N. Moll, R. Huber, J. Repp, Sub-cycle atomic-scale forces coherently control a single-molecule switch. *Nature* **585**, 58–62 (2020).
2. T. Kudernac, N. Ruangsupapichat, M. Parschau, B. Maciá, N. Katsonis, S. R. Harutyunyan, K.-H. Ernst, B. L. Feringa, Electrically driven directional motion of a four-wheeled molecule on a metal surface. *Nature* **479**, 208–211 (2011).
3. S. Mathias, S. Eich, J. Urbancic, S. Michael, A. V. Carr, S. Emmerich, A. Stange, T. Popmintchev, T. Rohwer, M. Wiesenmayer, A. Ruffing, S. Jakobs, S. Hellmann, P. Matyba, C. Chen, L. Kipp, M. Bauer, H. C. Kapteyn, H. C. Schneider, K. Rossnagel, M. M. Murnane, M. Aeschlimann, Self-amplified photo-induced gap quenching in a correlated electron material. *Nat. Commun.* **7**, 12902 (2016).
4. T. Rohwer, S. Hellmann, M. Wiesenmayer, C. Sohr, A. Stange, B. Slomski, A. Carr, Y. Liu, L. M. Avila, M. Källäne, S. Mathias, L. Kipp, K. Rossnagel, M. Bauer, Collapse of long-range charge order tracked by time-resolved photoemission at high momenta. *Nature* **471**, 490–493 (2011).
5. J. Madéo, M. K. L. Man, C. Sahoo, M. Campbell, V. Pareek, E. L. Wong, A. Al-Mahboob, N. S. Chan, A. Karmakar, B. M. K. Mariserla, X. Li, T. F. Heinz, T. Cao, K. M. Dani, Directly visualizing the momentum-forbidden dark excitons and their dynamics in atomically thin semiconductors. *Science* **370**, 1199–1204 (2020).
6. B. Shen, Y. Kim, M. Lee, Supramolecular Chiral 2D Materials and Emerging Functions. *Adv. Mater.* **32**, 1905669 (2020).
7. M. Gobbi, E. Orgiu, P. Samorì, When 2D Materials Meet Molecules: Opportunities and Challenges of Hybrid Organic/Inorganic van der Waals Heterostructures. *Adv. Mater.* **30**, 1706103 (2018).
8. R. J. D. Miller, Femtosecond crystallography with ultrabright electrons and x-rays: capturing chemistry in action. *Science* **343**, 1108–1116 (2014).
9. D. Curcio, S. Pakdel, K. Volckaert, J. A. Miwa, S. Ulstrup, N. Lanatà, M. Bianchi, D. Kutnyakhov, F. Pressacco, G. Brenner, S. Dziarzhyski, H. Redlin, S. Y. Agustsson, K. Medjanik, D. Vasilyev, H.-J. Elmers, G. Schönhense, C. Tusche, Y.-J. Chen, F. Speck, T. Seyller, K. Bühlmann, R. Gort, F. Diekmann, K. Rossnagel, Y. Acremann, J. Demsar, W. Wurth, D. Lizzit, L. Bignardi, P. Lacovig, S. Lizzit, C. E. Sanders, P. Hofmann, Ultrafast electronic linewidth broadening in the C 1s core level of graphene. *Phys. Rev. B* **104**, L161104 (2021).
10. D. Curcio, K. Volckaert, D. Kutnyakhov, S. Y. Agustsson, K. Bühlmann, F. Pressacco, M.

- Heber, S. Dziarzhytski, Y. Acremann, J. Demsar, W. Wurth, C. E. Sanders, P. Hofmann, Tracking the surface atomic motion in a coherent phonon oscillation. *Phys. Rev. B* **106**, L201409 (2022).
11. R. Wallauer, M. Raths, K. Stallberg, L. Münster, D. Brandstetter, X. Yang, J. Güdde, P. Puschnig, S. Soubatch, C. Kumpf, F. C. Bocquet, F. S. Tautz, U. Höfer, Tracing orbital images on ultrafast time scales. *Science* **371**, 1056–1059 (2021).
 12. K. Baumgärtner, M. Reuner, C. Metzger, D. Kutnyakhov, M. Heber, F. Pressacco, C.-H. Min, T. R. F. Peixoto, M. Reiser, C. Kim, W. Lu, R. Shayduk, M. Izquierdo, G. Brenner, F. Roth, A. Schöll, S. Molodtsov, W. Wurth, F. Reinert, A. Madsen, D. Popova-Gorelova, M. Scholz, Ultrafast orbital tomography of a pentacene film using time-resolved momentum microscopy at a FEL. *Nat. Commun.* **13**, 2741 (2022).
 13. C. W. Nicholson, A. Lücke, W. G. Schmidt, M. Puppig, L. Rettig, R. Ernstorfer, M. Wolf, Beyond the molecular movie: Dynamics of bands and bonds during a photoinduced phase transition. *Science* **362**, 821–825 (2018).
 14. D. Kutnyakhov, R. P. Xian, M. Dendzik, M. Heber, F. Pressacco, S. Y. Agustsson, L. Wenthaus, H. Meyer, S. Gieschen, G. Mercurio, A. Benz, K. Bühlman, S. Däster, R. Gort, D. Curcio, K. Volckaert, M. Bianchi, Ch. Sanders, J. A. Miwa, S. Ulstrup, A. Oelsner, C. Tusche, Y.-J. Chen, D. Vasilyev, K. Medjanik, G. Brenner, S. Dziarzhytski, H. Redlin, B. Manschwetus, S. Dong, J. Hauer, L. Rettig, F. Diekmann, K. Rosnagel, J. Demsar, H.-J. Elmers, Ph. Hofmann, R. Ernstorfer, G. Schönhense, Y. Acremann, W. Wurth, Time- and momentum-resolved photoemission studies using time-of-flight momentum microscopy at a free-electron laser. *Rev. Sci. Instrum.* **91**, 013109 (2020).
 15. D. Dattler, G. Fuks, J. Heiser, E. Moulin, A. Perrot, X. Yao, N. Giuseppone, Design of Collective Motions from Synthetic Molecular Switches, Rotors, and Motors. *Chem. Rev.* **120**, 310–433 (2020).
 16. K.-H. Ernst, Amplification of chirality in two-dimensional molecular lattices. *Curr. Opin. Colloid Interface Sci.* **13**, 54–59 (2008).
 17. Z. Hu, Z. Wu, C. Han, J. He, Z. Ni, W. Chen, Two-dimensional transition metal dichalcogenides: interface and defect engineering. *Chem. Soc. Rev.* **47**, 3100–3128 (2018).
 18. J. Lin Zhang, J. Qiang Zhong, J. Dan Lin, W. Ping Hu, K. Wu, G. Qin Xu, A. T. S. Wee, W. Chen, Towards single molecule switches. *Chem. Soc. Rev.* **44**, 2998–3022 (2015).
 19. J. Kügel, M. Leisegang, M. Bode, Imprinting Directionality into Proton Transfer Reactions of an Achiral Molecule. *ACS Nano* **12**, 8733–8738 (2018).
 20. Supplementary information.
 21. F. Roth, M. Borgwardt, L. Wenthaus, J. Mahl, S. Palutke, G. Brenner, G. Mercurio, S. Molodtsov, W. Wurth, O. Gessner, W. Eberhardt, Direct observation of charge separation in an organic light harvesting system by femtosecond time-resolved XPS. *Nat. Commun.* **12**, 1196 (2021).

22. I. Kröger, B. Stadtmüller, C. Wagner, C. Weiss, R. Temirov, F. S. Tautz, C. Kumpf, Modeling intermolecular interactions of physisorbed organic molecules using pair potential calculations. *J. Chem. Phys.* **135**, 234703 (2011).
23. L. Lyu, M. Mahalingam, S. Mousavion, S. Becker, H. Huang, M. Aeschlimann, B. Stadtmüller, Thermal-Driven Formation of 2D Nanoporous Networks on Metal Surfaces. *J. Phys. Chem. C* **123**, 26263–26271 (2019).
24. J. Felter, M. Franke, J. Wolters, C. Henneke, C. Kumpf, Two-dimensional growth of dendritic islands of NTCDA on Cu(001) studied in real time. *Nanoscale* **11**, 1798–1812 (2019).
25. G. Laurent, D. Lacoste, P. Gaspard, Emergence of homochirality in large molecular systems. *Proc. Natl. Acad. Sci. USA* **118**, e2012741118 (2021).
26. H. Karacuban, M. Lange, J. Schaffert, O. Weingart, Th. Wagner, R. Möller, Substrate-induced symmetry reduction of CuPc on Cu(111): An LT-STM study. *Surf. Sci.* **603**, L39–L43 (2009).
27. K. Schönauer, S. Weiss, V. Feyer, D. Lüftner, B. Stadtmüller, D. Schwarz, T. Sueyoshi, C. Kumpf, P. Puschnig, M. G. Ramsey, F. S. Tautz, S. Soubatch, Charge transfer and symmetry reduction at the CuPc/Ag(110) interface studied by photoemission tomography. *Phys. Rev. B* **94**, 205144 (2016).
28. A. Mugarza, N. Lorente, P. Ordejón, C. Krull, S. Stepanow, M.-L. Bocquet, J. Fraxedas, G. Ceballos, P. Gambardella, Orbital Specific Chirality and Homochiral Self-Assembly of Achiral Molecules Induced by Charge Transfer and Spontaneous Symmetry Breaking. *Phys. Rev. Lett.* **105**, 115702 (2010).
29. O. Stetsovych, M. Švec, J. Vacek, J. V. Chocholoušová, A. Jančařík, J. Rybáček, K. Kosmider, I. G. Stará, P. Jelínek, I. Starý, From helical to planar chirality by on-surface chemistry. *Nat. Chem.* **9**, 213–218 (2017).
30. R. Fasel, J. Wider, C. Quitmann, K.-H. Ernst, T. Greber, Determination of the Absolute Chirality of Adsorbed Molecules. *Angew. Chem. Int. Ed.* **43**, 2853–2856 (2004).
31. H. Cao, S. De Feyter, Amplification of chirality in surface-confined supramolecular bilayers. *Nat. Commun.* **9**, 3416 (2018).
32. M. Heber, N. Wind, D. Kutnyakhov, F. Pressacco, T. Arion, F. Roth, W. Eberhardt, K. Rossnagel, Multispectral time-resolved energy–momentum microscopy using high-harmonic extreme ultraviolet radiation. *Rev. Sci. Instrum.* **93**, 083905 (2022).
33. F. Aquilante et al., Molcas 8: New capabilities for multiconfigurational quantum chemical calculations across the periodic table, *J. Comput. Chem.* **37**, 506 (2016).
34. P. A. Malmqvist, A. Rendell, and B. O. Roos, The restricted active space self-consistent-field method, implemented with a split graph unitary group approach, *J. Phys. Chem.* **94**,

5477 (1990).

35. F. Haidu, G. Salvan, D. R. T. Zahn, L. Smykalla, M. Hietschold, M. Knupfer, Transport band gap opening at metal–organic interfaces. *J. Vac. Sci. Technol. A* **32**, 040602 (2014).
36. Davidson, E. R., Ortiz, J. V., and Staroverov, V. N. Complete-active-space extended Koopmans theorem method. *J. Chem. Phys.* **155**, 051102 (2021).
37. F. Evangelista, A. Ruocco, R. Gotter, A. Cossaro, L. Floreano, A. Morgante, F. Crispoldi, M. G. Betti, C. Mariani, Electronic states of CuPc chains on the Au(110) surface. *J. Chem. Phys.* **131**, 174710 (2009).
38. K. Niki, M. Nozaki, S. Kurihara, N. Komiya, Development of Analysis Method for Adsorption Site of Organic Molecule Determination Using Wave Number Space Resolved Photoelectron Spectroscopy. *Vacuum and Surface Science* **63**, 336–342 (2020).
39. M. Frisch, G. W. Trucks, Hb. Schlegel, G. E. Scuseria, M. A. Robb, J. R. Cheeseman, J. A. Montgomery Jr, T. Vreven, K. N. Kudin, Jc. Burant, Gaussian 03, revision c. 02; Gaussian. Inc., Wallingford, CT. **4** (2004).
40. O. D. Gordan, M. Friedrich, D. R. T. Zahn, The anisotropic dielectric function for copper phthalocyanine thin films. *Org. Electron.* **5**, 291–297 (2004).
41. M. Porer, U. Leierseder, J.-M. Ménard, H. Dachraoui, L. Mouchliadis, I. E. Perakis, U. Heinzmann, J. Demsar, K. Rossnagel, R. Huber, Non-thermal separation of electronic and structural orders in a persisting charge density wave. *Nat. Mater.* **13**, 857–861 (2014).
42. M. Rösner, E. Şaşıoğlu, C. Friedrich, S. Blügel, T. O. Wehling, Wannier function approach to realistic Coulomb interactions in layered materials and heterostructures. *Phys. Rev. B* **92**, 085102 (2015).
43. K. Andersen, S. Latini, K. S. Thygesen, Dielectric Genome of van der Waals Heterostructures. *Nano Lett.* **15**, 4616–4621 (2015).

Acknowledgements: The authors would like to thank Holger Meyer and Sven Gieschen for instrumentation support, and Bernhard Mahlmeister for his contribution to Fig. 1.

Funding: KB, CM and FR acknowledge financial support by the Deutsche Forschungsgemeinschaft (DFG) through the Würzburg-Dresden Cluster of Excellence ct.qmat (EXC 2147, project id 390858490). MR and DP-G acknowledge the support of the Volkswagen Foundation. MR and DP-G acknowledges support from the Cluster of Excellence 'CUI: Advanced Imaging of Matter' of the Deutsche Forschungsgemeinschaft (DFG) - EXC 2056 - project ID 390715994. DP-GMN acknowledges the student dispatch program by the Japan Student Services Organization (JASSO). MN, MH and KN thank the Supercomputer Center, the Institute for Solid State Physics and the University of Tokyo for the use of their facilities and acknowledge financial support from the Grants-in-Aid for Scientific Research (C) (No.20K05643) from Japan Society for the Promotion of Science and the Initiative for Realizing Diversity in the Research Environment of Chiba University. TW acknowledges support by the Cluster of Excellence 'CUI' of the DFG (EXC 2056, project ID 390715994). NW, MH, DK, SM and KR acknowledge financial support from the DFG (SFB 925, project ID 170620586).

Author contributions: MS designed the experiment. MS, KB, CM performed the data analysis. MN, MH, MR, KH, DP-G, TW, KN performed the theoretical study. MS, KB, NW, MH, DK, FP, LW, CHM and SM, conducted the experiment. MS, KB, and KR wrote the manuscript. MS, KB, MN, MR, NW, MH, MH, DK, FP, LW, KH, CHM, MB, FR, FR, AM, SM, TW, KN, DPG and KR contributed to scientific discussions.

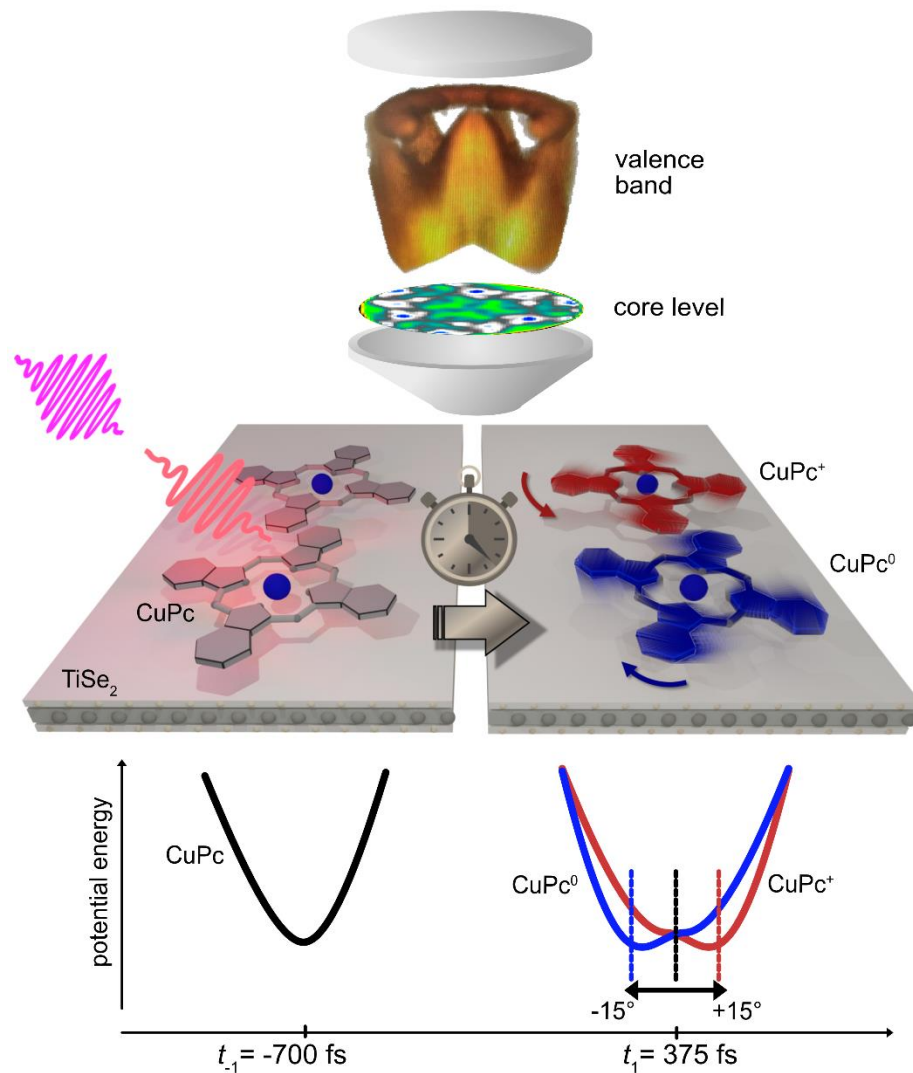


Fig. 1. Charge transfer-induced large-scale switching motions of adsorbed molecules.

Schematic illustration of the experimental results: The four-dimensional data sets of the valence band and core level regions of CuPc/TiSe₂ allow for capturing the large-scale rotational motion of the adsorbate on a sub-picosecond time scale. The rotations are triggered by changes in the surface potential following charge carrier transfer between TiSe₂ and CuPc and are in opposite directions for charged (red) and neutral (blue) molecules.

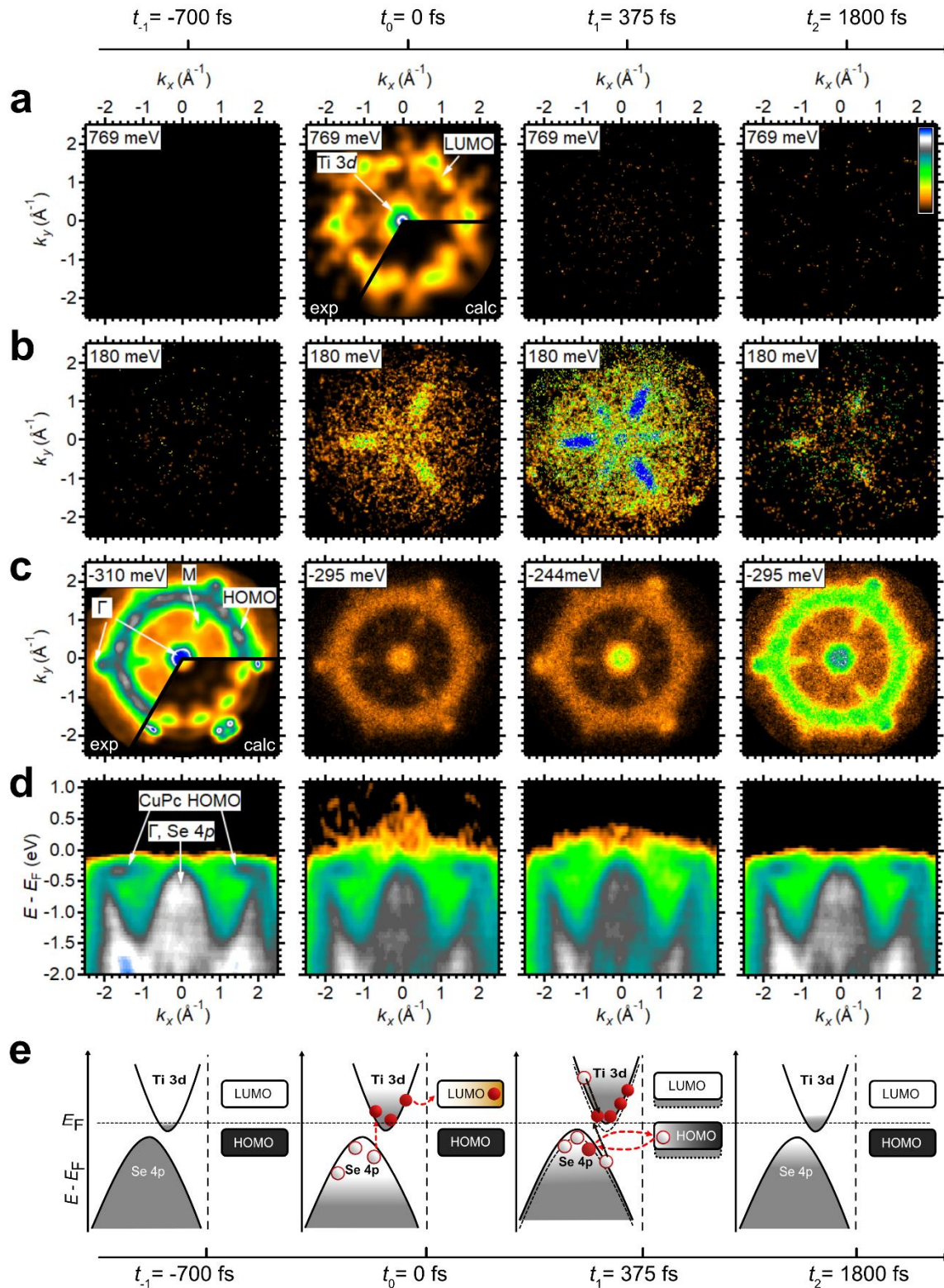


Fig. 2. Molecular movie of CuPc adsorbed on TiSe₂ resolved in energy-momentum space and time. Time-dependent momentum maps as well as energy-momentum maps at selected energies in the valence region at four delay times t_{-1} , t_0 , t_1 and t_2 (left to right). (a) LUMO, (b) Ti 3d conduction band, (c) HOMO, (d) valence band region. (e) Sketch of charge transfer dynamics between CuPc and TiSe₂.

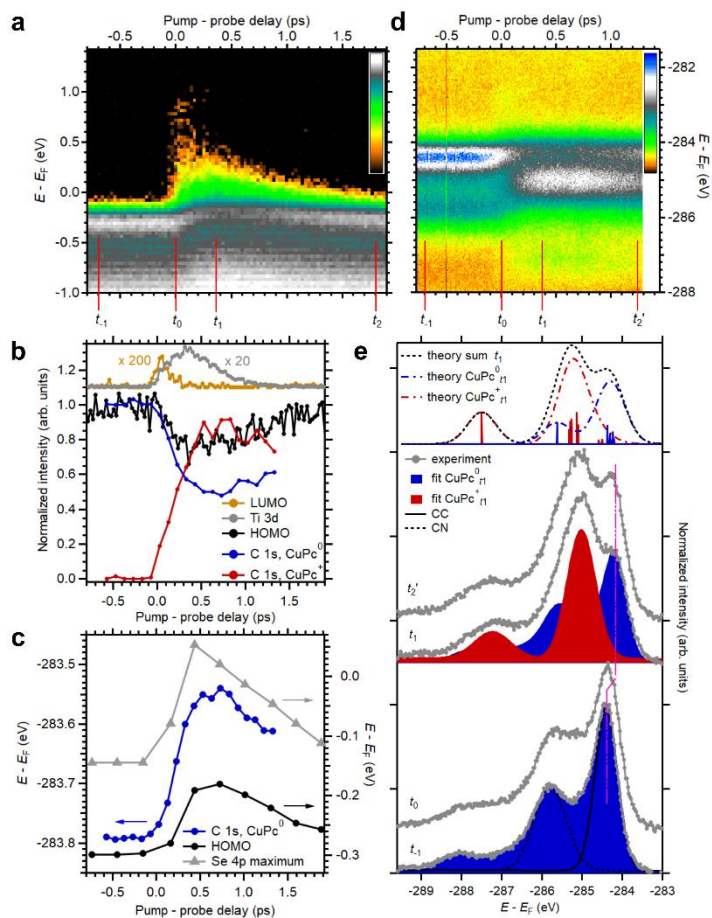


Fig. 3. Interfacial electronic dynamics. (a) Time-dependent photoemission spectrum of the CuPc/TiSe₂ valence region. (b) Transient normalized intensities of the CuPc LUMO (light brown), HOMO (black), the C 1s core level of neutral (blue) and charged (red) molecules, and the Ti 3d states of the substrate (gray). (c) Transient binding energy of the C 1s level of neutral molecules (blue), the HOMO (black), and the Se 4p maximum of the substrate (gray). (d) Transient spectrum of the C 1s core level. (e) C 1s spectra at t_{-1} , t_0 , t_1 and t_2' (from bottom to top, marked in (c)) including fits of the signatures of neutral (blue) and charged (red) molecules and the corresponding simulations (dashed lines).

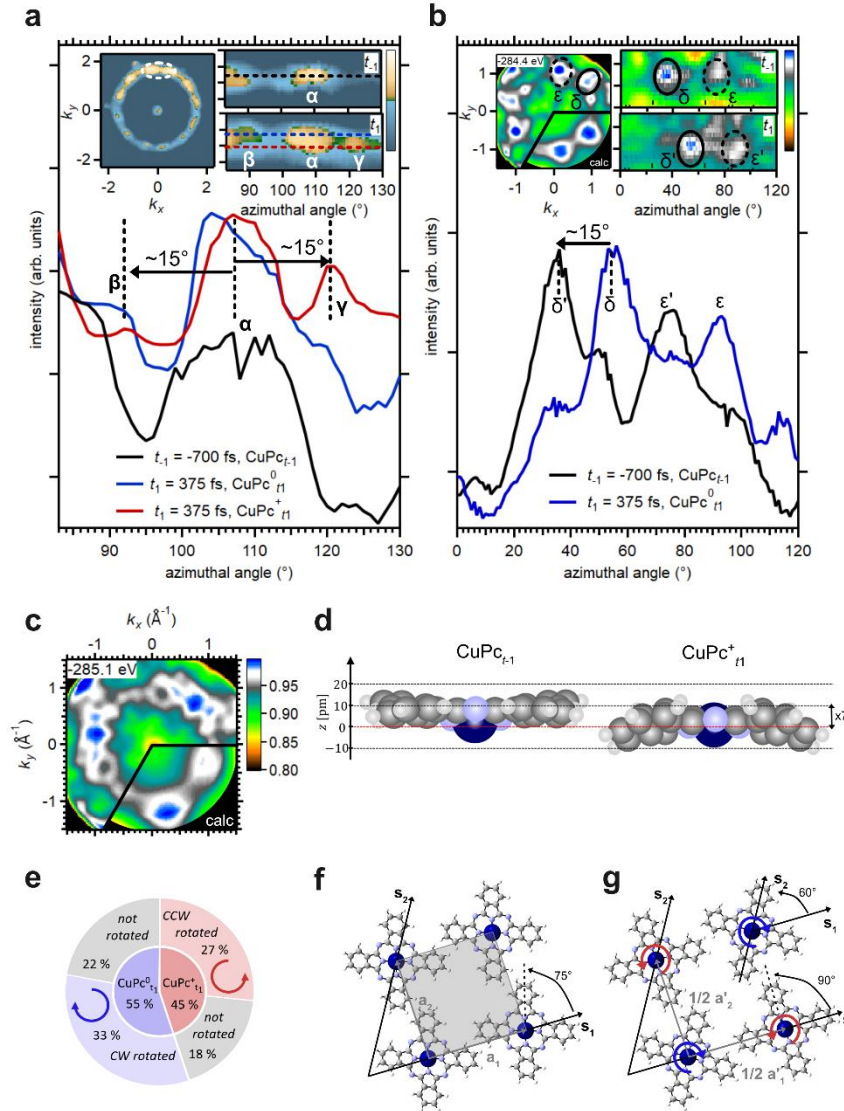
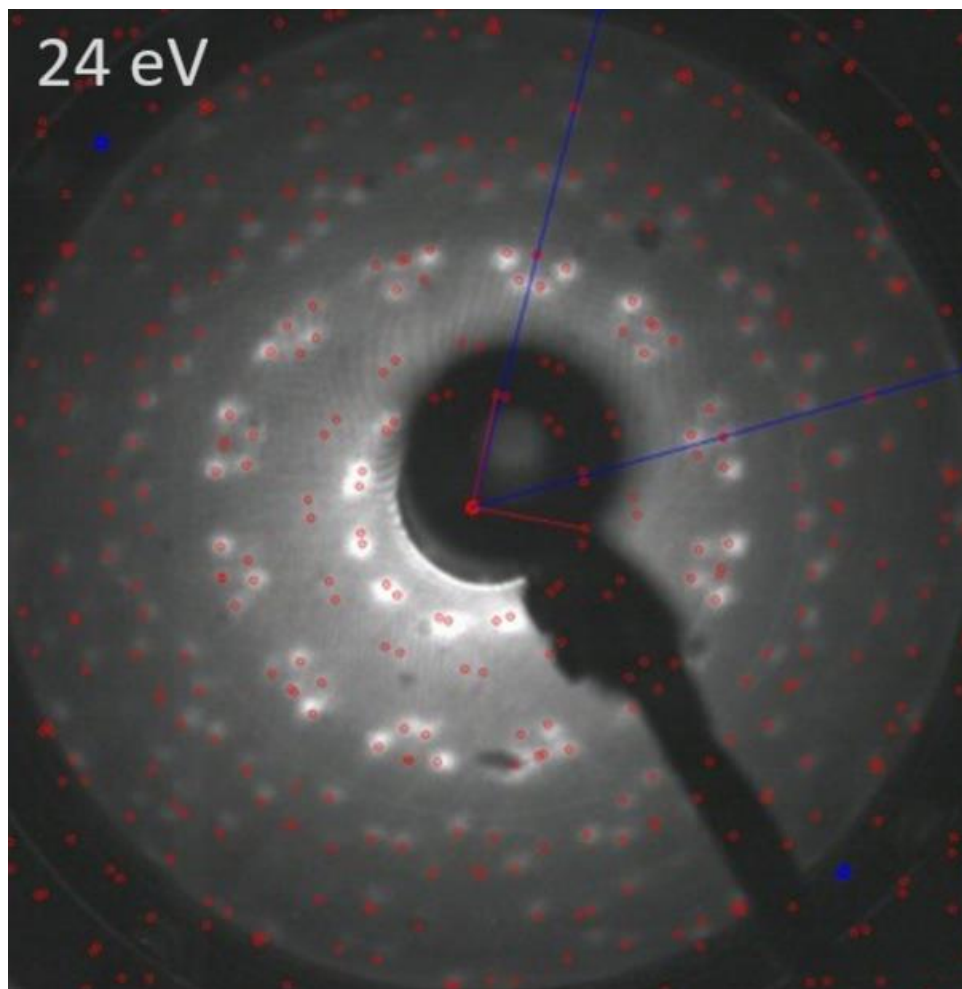
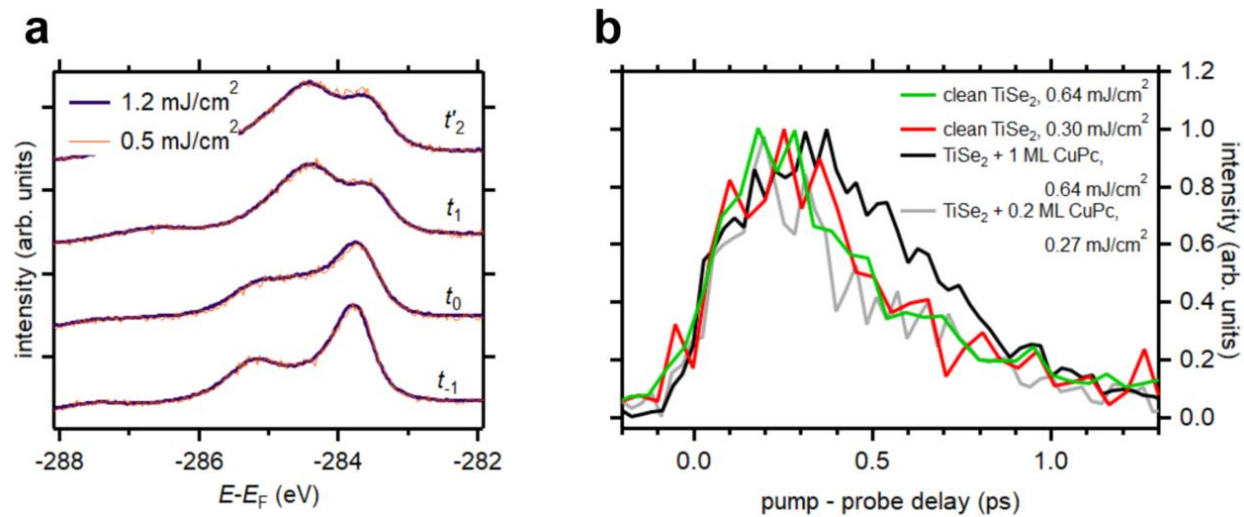


Fig. 4. Molecular structural dynamics. (a) Structural dynamics extracted from the CuPc HOMO momentum distribution. Azimuthal linecuts along the dashed lines marked in the inlays show the appearance of additional features (β , γ) at t_1 , separated by $\sim 15^\circ / +15^\circ$ from the HOMO features (α) at t_{-1} . (b) Rotation of $\text{CuPc}_{t_1}^+$ by $\sim -15^\circ$ extracted from the shift of the $\delta \rightarrow \delta'$ and $\varepsilon \rightarrow \varepsilon'$ features in the C 1s level at t_1 . (c) Comparison of the C 1s level of $\text{CuPc}_{t_1}^+$ with theory reveals a rotation of $\sim +15^\circ$. (d) Structural models extracted from the XPD pattern for CuPc and $\text{CuPc}_{t_1}^+$. Atomic diameters are scaled by a factor of 1/7. (e) Percentage of $\text{CuPc}_{t_1}^0$, $\text{CuPc}_{t_1}^+$, CW, CCW, and nonrotated molecules. (f, g) Sketch of the molecular arrangements at t_{-1} and t_1 , respectively.



Extended Data Fig. 1: LEED image of a monolayer of CuPc adsorbed on TiSe₂ ($E_{\text{kin}} = 24$ eV). The molecule derived reflexes are marked with red dots and the substrate spots are marked with blue dots. The lines indicate one symmetry set of the respective reciprocal lattices.



Extended Data Fig. 3: Fluence-dependent dynamics. (a) C 1s core level evolution of TiSe₂ covered by a monolayer CuPc for varying pump laser fluences. (b) Population dynamics of the Ti 3d conduction band for varying pump laser fluence for pristine TiSe₂, TiSe₂ covered by ~0.2 monolayers of CuPc, and TiSe₂ covered by a monolayer of CuPc.